A Thickness and Enthalpy Distribution Sea-Ice Model

JINLUN ZHANG AND DREW ROTHROCK

Polar Science Center, Applied Physics Laboratory, College of Ocean and Fishery Sciences, University of Washington, Seattle, Washington

(Manuscript received 5 June 2000, in final form 12 March 2001)

ABSTRACT

The theory of sea ice thickness distribution developed by Thorndike et al. has been extended to include sea ice enthalpy distribution. The extended theory conserves both ice mass and thermal energy, in the form of the heat stored in the ice, by jointly solving a thickness-distribution equation and an enthalpy-distribution equation. Both equations have been implemented in a one-dimensional dynamic thermodynamic sea-ice model with 12 ice thickness categories following the numerical procedure of Hibler. The implementation of the enthalpy-distribution equation allows the sea-ice model to account for any changes in the ice thermal energy induced by sea ice processes. As a result, the model is able to conserve not only the ice mass but also its thermal energy in the presence of ice advection, growth, melting, and ridging. Conserving ice thermal energy in a thickness-distribution sea ice model improves the prediction of ice growth, summer ice melt in particular, and therefore ice thickness. Inability to conserve the thermal energy by not implementing the enthalpy-distribution equation, compounded with an effect of the surface albedo feedback, causes the model to underestimate ice thickness by up to 11% under various conditions of thermal and mechanical forcing. This indicates the importance of conserving energy in numerical investigations of climate.

1. Introduction

Sea ice in the polar oceans plays a significant role in the changing earth climate system. The presence of sea ice drastically alters the air–sea exchange and therefore the atmospheric and oceanic circulations. The climatic importance of sea ice has motivated researchers to improve large-scale sea-ice models by incorporating more realistic sea-ice dynamics and thermodynamics. The status of sea-ice models and model development has been given in a number of recent overviews (e.g., Randall et al. 1998; Steele and Flato 2000). One of the widely used dynamic thermodynamic sea-ice models for climate studies is the Hibler (1979) model. This model and its variations are based on an idealized two-category representation of ice thickness that treats ice either as thick ice or as open water. To capture the behavior of sea ice with its variety of thicknesses, it is desirable to incorporate a thickness-distribution model with multiple ice thickness categories. Since Thorndike et al. (1975) presented the theory of sea-ice thickness distribution, an increasing number of researchers have started to use thickness-distribution models to study the polar climate (e.g., Hibler 1980; Flato and Hibler 1995; Schramm et al. 1997; Zhang et al. 1998b, 2000; Bitz et al. 2000). It is expected that in the future thickness-distribution models will also be incorporated into global climate models for climate studies on a global scale.

In the Thorndike et al. thickness-distribution theory the ice mass conservation is described by a single thickness-distribution equation (also see Hibler 1980),

$$\frac{\partial g}{\partial t} = -\nabla \cdot (\mathbf{u}g) - \frac{\partial (fg)}{\partial h} + F_L + \psi, \qquad (1)$$

where g is the ice-thickness distribution function, t is time, $\mathbf{u}$ is the ice velocity ($\mathbf{u} = u\mathbf{i} + v\mathbf{j}$), $\mathbf{i}$ and $\mathbf{j}$ are unit x–y vectors, f is the ice growth rate, h is the ice thickness, F_L is a source term for lateral melting, and ψ is a redistribution function for ridging. Equation (1) represents an Eulerian description of ice thickness distribution, not only in physical space (x–y space) but also in the ice thickness variable h. In such an Eulerian model, the third independent coordinate is ice thickness h, and (1) is therefore an equation for g in a three-dimensional (x–y–h) space. Thorndike et al. (1975) also presented a Lagrangian thickness distribution equation [their Eq. (16)], which is different from the Eulerian equation (1) in form and is solved following the characteristics that are determined by $d\mathbf{r}/dt = \mathbf{u}$ ($\mathbf{r} = x\mathbf{i} + y\mathbf{j}$) and $dh/dt = f$ in (x–y–h, t) space. Recently, Bitz et al. (2001) presented a thickness distribution sea-ice model, which is Eulerian in x–y space and Lagrangian in h domain. Their model solves two equations to de-

Corresponding author address: Dr. Jinlun Zhang, Polar Science Center, Applied Physics Laboratory, College of Ocean and Fishery Sciences, University of Washington, 1013 NE 40th Street, Seattle, WA 98105-6698.
E-mail: zhang@apl.washington.edu

termine ice thickness distribution, one for ice concentration and the other for ice volume per unit area.

Different from the approach of Bitz et al. (2001), the present study focuses on the Thorndike et al. Eulerian thickness distribution equation (1), first implemented by Hibler (1980) in a large-scale, dynamic thermodynamic sea-ice model with multiple ice thickness categories. The multicategory thickness-distribution model explicitly simulates the ice ridging process, allows a fine-resolution calculation of ice thermodynamic growth and decay for each thickness category, and therefore captures the essence of the coupling of the dynamic and thermodynamic sea ice processes better than the two-category models. The model has been used in recent years for large-scale arctic climate studies and has proven able to realistically simulate large-scale variability in ice motion, thickness distribution, and ridging (Flato and Hibler 1995; Zhang et al. 1998b, 2000; Arbetter et al. 1999). The Hibler (1980) thickness-distribution sea-ice model has been improved by Flato and Hibler (1995), who also investigated its sensitivity to the mechanical parameters in the ice thickness distribution. The improved model simulates the evolution of snow by solving a snow-thickness distribution equation.

This paper focuses on the representation of thermodynamics. The Hibler and Flato–Hibler models use the so called zero-layer thermodynamic model of Semtner (1976) to estimate ice growth or decay for each ice category by simplifying and solving the following ice heat equation:

$$\rho c_p \frac{\partial T}{\partial t} = \frac{\partial}{\partial z} k \frac{\partial T}{\partial z} + \kappa I e^{-\kappa z}, \tag{2}$$

where ρ ($=905$ kg m^{-3}) is ice density, c_p ($=2100$ J kg^{-1} K^{-1}) is ice heat capacity, z is ice depth (measured positive upward from the bottom of the ice), T is ice temperature, k ($=2.03$ W m^{-1} K^{-1}) is ice conductivity, κ ($=1.5$ m^{-1}) is the bulk shortwave extinction coefficient of sea ice, and I ($=0.3$) is the penetration of solar radiation at the ice surface. The zero-layer thermodynamic model assumes that ice does not store heat and, therefore, tends to exaggerate the seasonal variability in ice thickness. The exaggeration, however, can be significantly reduced by using the three-layer thermodynamic model of Semtner (1976), which allows ice to store heat. Semtner (1976) concluded that under a wide variety of environmental conditions, the seasonal variations in ice thickness simulated using the three-layer approximation to (2) compared well with a more complete numerical solution of (2) with more ice layers (Maykut and Untersteiner 1971).

Recently, the three-layer thermodynamic model has been reformulated by Winton (2000). The reformulation improves the model physics by representing the brine content of the upper ice with a variable heat capacity. It also improves the model numerics so that it consumes less computer time and memory. Consequently, the Winton three-layer model is a suitable candidate for replacing the zero-layer model in Hibler's multicategory thickness-distribution sea-ice model. Of course, a general multilayer thermodynamic model, such as that of Maykut and Untersteiner (1971) and its variations (e.g., Ebert and Curry 1993; Flato and Brown 1996), may also be used to replace the zero-layer model if computer resources permit.

Since a three-layer thermodynamic model or a general multilayer model allows ice to store heat, it is desirable to conserve the stored heat (also called enthalpy or thermal energy). Not conserving thermal energy in the ice is likely to cause errors in estimating ice growth and decay and the timing of ice thaw and freeze-up. A key issue with multicategory thickness-distribution sea-ice models using a three-layer or a general multilayer thermodynamics is therefore the conservation of ice thermal energy in the presence of ice advection, growth, decay, lateral melting, and ridging. Needless to say, it is difficult to track thermal energy in the complicated ridging process (Bjork 1992). Another area of complication in conserving thermal energy is related to the fact that ice constantly shifts from one category to another owing to ice growth and decay. However, the issue of energy conservation needs to be resolved before implementing a three-layer or multilayer thermodynamic scheme in thickness-distribution models. Energy conservation is particularly necessary in long-term climate simulations and predictions.

The study reported here resolves the issues concerning the conservation of thermal energy in thickness-distribution sea-ice models. We introduce a sea ice enthalpy-distribution function and an associated enthalpy-distribution equation into the ice system. This enthalpy-distribution equation, in parallel with the thickness-distribution equation, allows the model to conserve ice thermal energy during all sea ice processes. The enthalpy-distribution theory is presented in section 2. Its numerical implementation in a thickness-distribution sea-ice model employing the Winton three-layer thermodynamics is presented in section 3. In section 4, output from the full thickness- and enthalpy-distribution model is compared to that from a model that does not implement the enthalpy distribution and therefore does not conserve enthalpy and to that from a model that employs the zero-layer thermodynamics and therefore does not allow ice to store enthalpy. Conclusions are given in section 5.

2. Theory of ice enthalpy distribution

Before introducing ice enthalpy distribution we first define ice enthalpy per unit area, H, such that

$$H(x, y, h, t) = \int_0^h \rho c_p T(x, y, z, h, t)\, dz, \tag{3}$$

where T is ice temperature. Equation (3) determines the whole thermal energy in a unit area of pack ice with

thickness h. The ice enthalpy distribution function, e, is defined as the product of ice enthalpy per unit area and ice thickness distribution and is written as

$$e(x, y, h, t) = g(x, y, h, t)H(x, y, h, t). \quad (4)$$

This is a non-normalized distribution function, unlike the thickness distribution function, which is a normalized function. Obviously, the enthalpy-distribution function gives a full picture of the heat content of ice of different thicknesses and areal fractions such that $e(h)dh$ represents the thermal energy of ice of thickness h. The thermal energy of ice thinner than h can be determined by a cumulative enthalpy-distribution function, defined as $E(x, y, h, t) = \int_0^h e(x, y, h', t)\, dh'$, and $E(x, y, \infty, t)$ is the total thermal energy per unit area in all ice categories.

Like thickness distribution, enthalpy distribution is subject to changes brought about by ice advection, thermodynamic growth or decay, lateral melting, and ridging. In order to conserve ice thermal energy, these processes must be accounted for in an enthalpy conservation equation. If we define $\mathbf{u}e$ as a flux of enthalpy distribution in the physical x–y space, we find that the change in enthalpy distribution due to ice advection is equal to the negative divergence of the flux, $-\nabla \cdot (\mathbf{u}e)$, following the same argument as given by Thorndike et al. (1975). Similarly, if we define fe as a flux of enthalpy distribution in the h domain, the negative divergence of the flux, $-\partial(fe)/\partial h$, is the change in enthalpy distribution due to ice growth. Note that lateral melting, F_L, does not cause ice to transfer from one category to another (Hibler 1980). Therefore, the change due to lateral melting can be easily found to be HF_L. Now if we define Φ as an enthalpy redistribution function that represents the change in enthalpy distribution due to the mechanical ridging process, then we have the governing equation for the enthalpy distribution:

$$\frac{\partial e}{\partial t} = -\nabla \cdot (\mathbf{u}e) - \frac{\partial(fe)}{\partial h} + HF_L + \Phi. \quad (5)$$

The enthalpy redistribution function Φ must meet two requirements. First, it must track the enthalpy in all ice thickness categories during the ridging process of transferring thinner ice to thicker ice. In order to do that, it must be closely linked to the thickness redistribution function ψ. Second, it must conserve the total enthalpy during ridging such that

$$\int_0^\infty \Phi\, dh = 0. \quad (6)$$

The thickness redistribution function is written as (Thorndike et al. 1975; Hibler 1980)

$$\psi = c_1\delta(h) + c_2\left[-P(h)g(h) + \int_0^\infty \gamma(h', h)P(h')g(h')\, dh'\right], \quad (7)$$

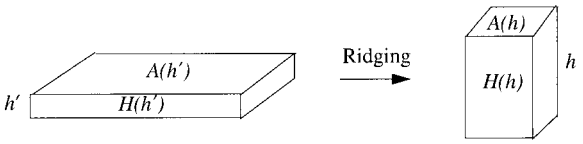

FIG. 1. Illustration of how thin ice of thickness h', area $A(h')$, and enthalpy per unit area $H(h')$ is transferred into thicker ice of thickness h, area $A(h)$, and enthalpy per unit area $H(h)$ owing to ridging.

where

$$c_1 = (P^*)^{-1}\sigma_{ij}\dot{\varepsilon}_{ij} + \dot{\varepsilon}_{kk},$$

$$c_2 = \frac{(P^*)^{-1}\sigma_{ij}\dot{\varepsilon}_{ij}}{\int_0^\infty \left[P(h)g(h) - \int_0^\infty \gamma(h', h)P(h')g(h')\, dh'\right] dh},$$

σ_{ij} is the ice stress tensor, $\dot{\varepsilon}_{ij}$ is the ice strain rate tensor, P^* is ice strength, P is a function specifying which categories of ice participate in ridging, and $\gamma(h', h)$ is a redistributor of the thickness distribution. The redistributor is formulated in such a way that $\gamma(h', h)dh$ can be thought of as the area of ice put into the thickness interval $[h, h + dh]$ when a unit area of ice of thickness h' is used up (Hibler 1980). For the Eulerian thickness-distribution equation, (1), $\gamma(h', h)$ is time independent and is given by Hibler (1980). In order to conserve ice mass, the ice thickness redistributor must meet the following constraint:

$$\int_0^\infty \gamma(h', h)h\, dh = h'. \quad (8)$$

The first term in (7) specifies the amount of open water created, which does not contribute to changes in the enthalpy distribution. The second term in (7) describes the transfer of thin ice to thick ice by ridging, which controls the changes in enthalpy distribution. It states that during ridging the category of ice thickness h contributes an areal fraction of $c_2P(h)g(h)$ to other categories and at the same time gains an areal fraction of $\int_0^\infty c_2\gamma(h', h)P(h')g(h')\, dh'$ from other categories. Assume now that an amount of ice of thickness h', area $A(h')$, and enthalpy per unit area $H(h')$ is ridged into a category of ice thickness h, area $A(h)$, and enthalpy per unit area $H(h)$, as shown in Fig. 1. The requirements for conserving both mass and enthalpy during the assumed ridging process are $A(h)h = A(h')h'$ and $A(h)H(h) = A(h')H(h')$, which leads to $H(h) = A(h')H(h')/A(h) = hH(h')/h'$. Assume further that the category of ice thickness h gains an areal fraction of $c_2\gamma(h', h)P(h')g(h')dh'$ from the category of ice thickness h', then its corresponding enthalpy gain is $H(h)c_2\gamma(h', h)P(h')g(h')dh'$, or $(h/h')c_2\gamma(h', h)P(h')e(h')dh'$, given that $e(h') = g(h')H(h')$. Thus, in summation of the contributions from all the categories, the enthalpy redistribution function can be conveniently written as

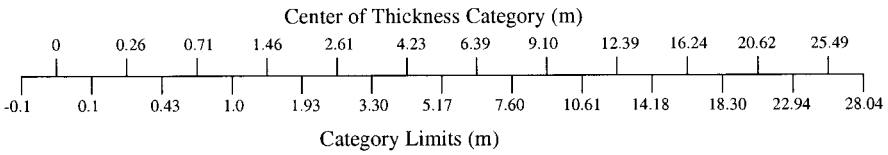

FIG. 2. Schematic arrangement of thickness partition used in the 12-category thickness- and enthalpy-distribution sea-ice model.

$$\Phi = c_2\left[-P(h)e(h) + \int_0^\infty \gamma(h', h)P(h')e(h')\frac{h}{h'}\,dh'\right]. \tag{9}$$

This equation captures all the enthalpy changes due to ridging. In addition, by taking (8) into account, it is easy to prove that Φ formulated in (9) satisfies (6) and therefore conserves enthalpy. Thus, the derivation of the governing equation of the enthalpy distribution, (5), is completed.

3. Numerical implementation of enthalpy distribution

a. Model description

In order to examine the effects of enthalpy conservation on modeling sea ice, we have implemented the enthalpy-distribution equation, (5), into a one-dimensional thickness-distribution sea-ice model. Although the model is one-dimensional, it takes into account the effects of ice divergence and shear on ice transport and ridging. The sea-ice model has 12 thickness categories, partitioned following a Gaussian distribution to obtain a thickness mesh that varies smoothly in space (Fig. 2). The 12-category ice thickness-distribution equation is solved following the Hibler (1980) finite-differencing procedure. The parameters governing the ridging process, such as the frictional dissipation coefficient, the ridge participation constant, and shear ridging parameter, are given by Flato and Hibler (1995; see their Table 3 for the standard case). The ice enthalpy-distribution equation, based on the same 12 ice categories, is solved following the same numerical procedure. Accompanying the ice model is a snow model described in terms of snow thickness distribution, $g_s(h)$, corresponding to the ice thickness distribution, $g(h)$. The treatment of the snow thickness distribution, the solution of the snow conservation equation, and the parameterization of surface albedo, dependent on the surface conditions of snow, ice, open water, and surface temperature, are described in detail by Flato and Hibler (1995; in their appendix and Table 2). The heat equation, (2), of the snow–ice system is solved using the Winton (2000) three-layer thermodynamic model, which divides the ice in each category into two layers of equal thickness beneath a layer of snow (Fig. 3) and calculates the surface temperature T_s, the upper ice temperature T_1, the lower ice temperature T_2, and the ice growth rate f.

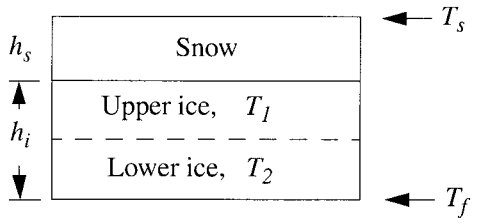

FIG. 3. Schematic representation of the Winton (2000) three-layer thermodynamic model. For each ice thickness category h_i, the model computes snow thickness h_s, upper ice temperature T_1, lower ice temperature T_2, and ice growth rate f. The temperature at the bottom of the ice is fixed at $T_f = -1.96$, the freezing temperature of seawater. The temperature at the surface of the ice or snow, T_s, is determined from a surface energy balance.

The solution of (2) provides a vertical profile of ice temperature that can be used to calculate the ice-enthalpy distribution based on (4). The enthalpy distribution is then updated by solving (5), which is in turn used to update ice temperatures T_1 and T_2. However, the variability of the upper ice temperature, T_1, is considerably different from that of the lower ice temperature, T_2 (see Figs. 11 and 14 in section 4c), and the updated enthalpy distribution defined by (3) and (4) may not give enough information to distinguish the temperature changes in the individual layers. To deal with this difficulty, we assume that changes in the ice enthalpy in each layer because of ice advection, growth or decay, and ridging are confined to the same layer. This assumption implies that, when ice transfers to a different thickness category owing to any of the processes, its upper and lower enthalpy would merge, respectively, with the upper and lower enthalpy of the ice in that category. Merging of enthalpy following this rule is certainly accurate with regard to ice advection. It may not be so accurate with regard to ice growth or decay and ridging, but it is unlikely to cause large errors. On the basis of this assumption, we can solve two enthalpy conservation equations similar to (5) in form, one for the upper enthalpy and the other for the lower enthalpy, and then update T_1 and T_2 separately. To simplify the solution, we allow the term ρc_p in (3) to be constant.

The solution procedure consists of the following steps:

1) Solve the sea-ice momentum equations (see, e.g., Hibler 1979) to obtain ice velocity, divergence, and shear. This step is not performed by the one-dimensional model used in this study; rather, it is per-

formed by a three-dimensional coupled ice–ocean model of Zhang et al. (1998b, 2000), whose daily outputs for ice velocity, divergence, and shear are used to drive the one-dimensional model (see details in section 3.2).

2) Solve the heat equation (2) of the snow–ice system using the Winton (2000) three-layer thermodynamic model. The ice enthalpy distribution is

$$e_1 = \rho c_p \frac{dh}{N} T_1$$

in the upper layer and

$$e_2 = \rho c_p \frac{gh}{N} T_2$$

in the lower layer, where $N = 2$.

3) Solve the ice thickness-distribution equation (1) by computing the changes in thickness distribution due to ice transport, ice growth or decay, lateral melting, and ridging, and obtain an updated thickness distribution g'.

4) Solve the snow-thickness distribution equation following the procedure of Flato and Hibler (1995) to obtain the snow depth for each ice thickness category.

5) Insert e_1 and e_2 separately into the enthalpy-distribution equation (5) to obtain two conservation equations; solve these two equations by computing the changes in enthalpy due to ice transport, ice growth or decay, lateral melting, and ridging and obtain an updated upper enthalpy distribution e_1' and a lower enthalpy distribution e_2'.

6) Update ice temperatures T_1' and T_2' according to

$$T_j' = Ne_j'/(\rho c_p g' h) \qquad j = 1, 2; \qquad N = 2. \quad (10)$$

Note that this procedure is also useful for models with general multilayer thermodynamics.

b. Forcing data

The model is driven by daily forcing data derived in 1996 for the North Pole area from observations and model outputs (as described below). The forcing data consist of geostrophic winds, air temperature 2 m above the surface, specific humidity, shortwave and longwave radiations, snow fall, oceanic heat flux, and ice velocity, divergence, and shear. The geostrophic winds at the North Pole are calculated using gridded sea level pressure (SLP) fields provided by I. G. Rigor from the International Arctic Buoy Program (IABP) (see Thorndike et al. 1983). The daily 2-m temperature data at the North Pole (Fig. 4a) are derived from buoys, manned drift stations, and all available land stations (Rigor et al. 2000; also see Martin and Munoz 1997). The specific humidity and longwave and shortwave radiative fluxes are calculated following the method of Parkinson and Washington (1979) based on the SLP and air temperature fields. The downward longwave and shortwave radiative fluxes are shown in Figs. 4b and 4c. Monthly varying snow fall rates for the North Pole area are from the Vowinckel and Orvig (1970) climatology, which are also listed by Zhang et al. (1998a) and Flato and Hibler (1995). These snowfall rates (water equivalent), in millimeters per month, for January through December, respectively, are 12.3, 5.6, 8.5, 2.2, 3.5, 11.1, 16.6, 23.4, 16.1, 14.5, 7.5, and 6.3. Oceanic heat flux is set to a constant 2 W m^{-2}.

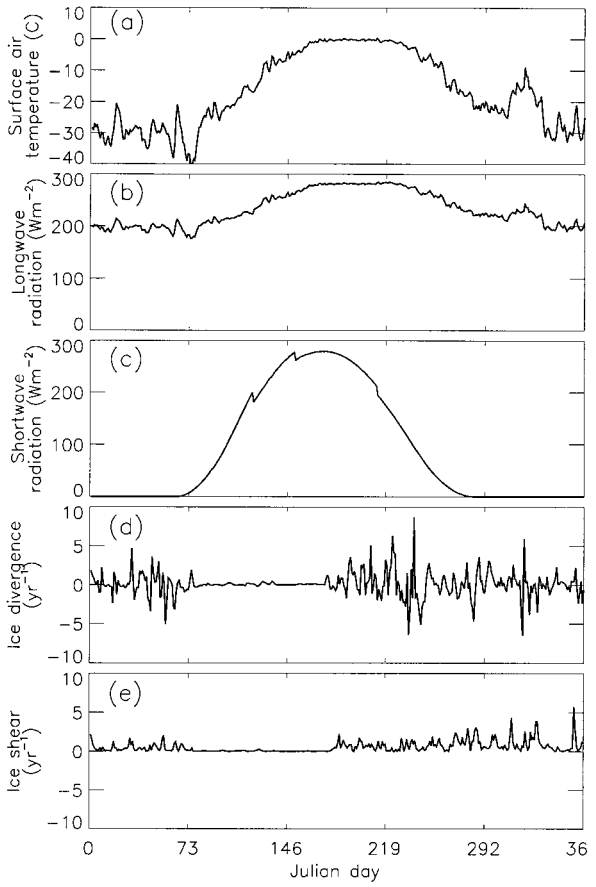

FIG. 4. Forcing data used to drive the sea-ice model. (a) Air temperature measured 2 m above the sea surface, (b) downward longwave radiation at the surface, (c) downward shortwave radiation at the surface, (d) ice divergence, and (e) ice shear at the North Pole. Data are for 1996 and were derived from observations and model outputs.

As mentioned earlier the daily ice velocity, divergence, and shear are calculated by a three-dimensional coupled ice–ocean model of the Arctic Ocean and the adjacent seas (Zhang et al. 1998b, 2000). The model has a 40-km horizontal resolution and has been continuously driven by the aforementioned daily forcing from 1979 to 1996. The model solves ice momentum equations associated with a viscous plastic ice rheology, using a line successive relaxation technique to obtain a better plastic solution for ice motion, deformation, and stress (Zhang and Hibler 1997). The 3D model's output of 1996 daily ice velocity, divergence, and shear at the

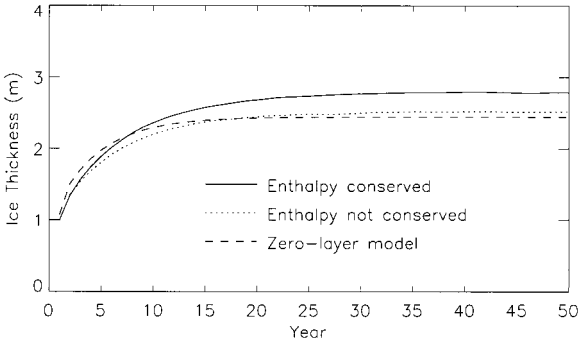

FIG. 5. Evolution of the simulated annual mean ice thickness.

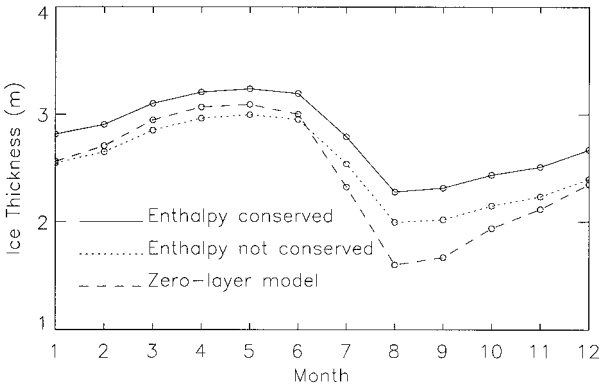

FIG. 6. Simulated monthly mean ice thickness.

North Pole (Figs. 4d and 4e) is used as forcing data to determine the ice transport, deformation, and ridging in the 1D model. Plotted in Figs. 4d and 4e, the modeled ice divergence and shear are generally small from mid-March through mid-June because of a thicker ice cover that is stronger and more resistant to deformation. In other seasons, the simulated divergence and shear have considerable fluctuations, which allow the 1D model to simulate ice opening or closing and ridging.

4. Results and discussion

The full thickness- and enthalpy-distribution sea-ice model was run for 50 yr repeatedly using the 1996 daily forcing. Unless stated otherwise, the results from the 50th yr are presented. In order to examine the effects of enthalpy conservation on the seasonal variability of sea ice, a second model was run in which (5) was not solved and therefore ice enthalpy was not conserved in the presence of ice advection, growth and decay, and ridging. In addition, a third model was also run in which the zero-layer thermodynamic scheme was used. The third model was included to examine the effects of different thermodynamic schemes, whether or not they allowed ice to store heat, when they were implemented in multicategory thickness-distribution sea-ice models. For convenience hereafter, the first model is referred to as the enthalpy-conserving model or full model, the second model is referred to as the nonconservative model, and the third model is referred to as the zero-layer model.

a. Ice thickness

Figure 5 shows the 50-yr evolution of mean ice thickness $\int_0^\infty g(h)h\,dh$ for the three models. All three model runs start at an initial condition of uniform 0.26-m-thick ice, which falls into ice category 2 (Fig. 2). After about 20 years of spinup, all the models reach a steady state. The zero-layer model does not allow heat storage in the ice and therefore approaches the steady state more rapidly than the other two models. The annual mean ice thickness at the 50th year is 2.79 m for the full model, 2.52 m for the nonconservative model, and 2.45 m for the zero-layer model. The difference in the annual mean ice thickness between the full model and the nonconservative model is 0.27 m, or 11%, which indicates that not conserving ice enthalpy is likely to cause a significant underestimation of ice thickness.

Although the nonconservative model and the zero-layer model do not differ significantly in the annual mean ice thickness (Fig. 5), they differ considerably in the seasonal variability of ice thickness (Fig. 6). The annual thickness range is 1.49 m for the zero-layer model, 1.00 m for the nonconservative model, and 0.96 m for the full model. Compared to the models that use the three-layer thermodynamic scheme, the zero-layer model substantially exaggerates the seasonal variation of ice thickness. The amplitude of the seasonal cycle is in error as a result of ignoring the storage of heat in ice. This is in line with the results of Semtner (1976). However, Semtner's results are based on a calculation of ice with a single thickness of around 3 m, whereas the results shown in Fig. 6 are based on simultaneous calculations of ice with a distribution of all thicknesses ranging from 0 to 28 m. This indicates that Semtner's conclusion about the errors induced by the zero-layer model is as applicable to a model with a thickness distribution as to a model with a single ice type.

Note that the seasonal cycles for the full and nonconservative models track each other very closely, with the nonconservative model thickness always being about 0.27 m thinner. The phase of the cycle—the timing of maximum and minimum—is very similar for the two models. As noted above, however, the annual mean computed by the full model is about 11% larger than that computed by the nonconservative model. This can be attributed to the models' different behaviors in simulating ice temperature and ice growth/melt and in responding to surface albedo feedback, which is to be presented in detail in the following sections.

The thickness distributions simulated by the full model are shown in Figs. 7a and 7b and compared to those simulated by the other two models in Figs. 7c and 7d. Since the models have 12 thickness categories, the dis-

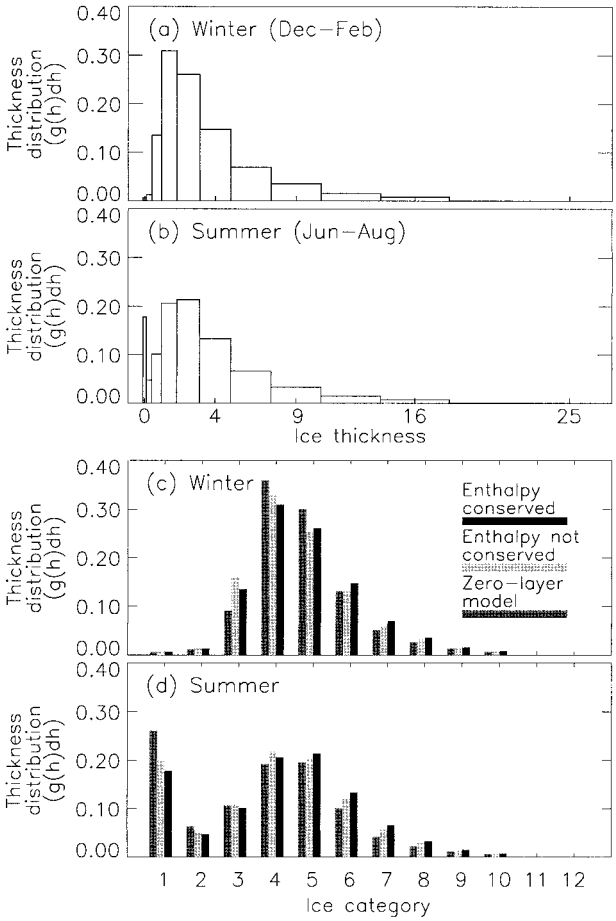

FIG. 7. Simulated mean ice-thickness distribution by the enthalpy-conserving model in (a) and (b) and comparison of thickness distributions among the three models in (c) and (d). The histograms in (a) and (b) are plotted over 12 bins corresponding, respectively, to the 12 ice-thickness categories shown in Fig. 2. They are plotted as distributions (units of m on the horizontal axis and area fraction on the vertical) so the area within a chosen bin represents the ice volume per unit area in the corresponding thickness interval.

tributions are plotted for 12 bins. As can be seen, the models simulate ice in a range of thicknesses owing to the ridging process driven by the daily divergence and shear forcing. Most of the simulated ice, however, is about 1–3 m thick (categories 4 and 5). In winter, all three models create about the same amount of open water (category 1 in Figs. 2, 7c, and 7d). The existence of open water, though small, is due to the existence of ice divergence and shear (Figs. 4d and 4e) that allow ice opening. The full model generally predicts more thick ice than the other two models, the nonconservative model predicts more 1–2 m ice (categories 3 and 4) than the full model, and the zero-layer model predicts more 2–3 m ice (categories 4 and 5) than either three-layer model. In summer, the 0.4–2 m ice decreases quickly, so the area of open water and very thin ice (0–0.4 m) grows rapidly, particularly in the zero-layer model. As a result, the models all show a summer thickness-distribution function with two peaks, one in the open water category and the other in the 1–3 m categories. Again, the full model predicts more thick ice than the other two models. It also predicts a smaller area of open water and thin ice (Fig. 7d).

b. Ice growth and melt

The exaggeration of seasonal cycle of ice thickness by the zero-layer model and the underestimation of mean ice thickness by the nonconservative model are expected to be linked to the models' behavior in estimating ice growth and melt. Figure 8 shows how the simulated ice growth rates vary with ice thickness. In winter, there is a huge ice growth over open water. The growth rates drop drastically for 0.4–1 m ice and then diminishes with increasing ice thickness (Fig. 8a). The growth rates estimated by the full model are about the same as those estimated by the nonconservative model, whereas the growth rates estimated by the zero-layer model are about 0.5 m yr^{-1} larger than those estimated by the other two models over all thicknesses (Fig. 8b).

In summer, ice melts across the board (Fig. 8c). Magnified in Fig. 8d, the melt rates calculated by the full model and the nonconservative model change sharply for 0.4–2 m ice and gradually for thicker ice. The melt rates calculated by the zero-layer model, on the other hand, stay essentially the same over all the ice categories. This is because the model treats ice as if it has no heat capacity, that is, as if it has a linear temperature gradient. This treatment allows ice of all thicknesses to respond immediately and similarly to any change in thermal forcing at the surface. The lack of heat capacity in the ice also causes the zero-layer model to predict substantially more summer melting, which ranges depending on ice thickness from 0.5 to 4 m yr^{-1} more than the other two models. This explains why the model tends to considerably exaggerate the seasonal cycle (Fig. 6).

The nonconservative model, in comparison with the enthalpy-conserving model, also predicts more summer melting but to a much lesser degree. The increase in the melt rate ranges from about 1 m yr^{-1} for thin ice to about 0.5 m yr^{-1} for very thick ice. Because of the increase in melting, the annual mean growth rate for the nonconservative model is slightly lower than that for the full model (Fig. 8f). Although the increase in melting only causes a slight increase in the seasonal variability of the ice thickness, over time it is responsible for an 11% underestimation of mean ice thickness (Fig. 5).

The seasonal variability in ice growth rate for different ice types is illustrated in Fig. 9. For open water and very thin ice (0–0.4 m), all three models simulate huge ice growth in winter, early spring, and fall (Fig. 9a). The melt season is limited to the summer three months (June–August). The difference among the three models is small relative to the large values of the growth rates. This is no surprise since the zero-layer thermodynamic model is expected to be almost equivalent to

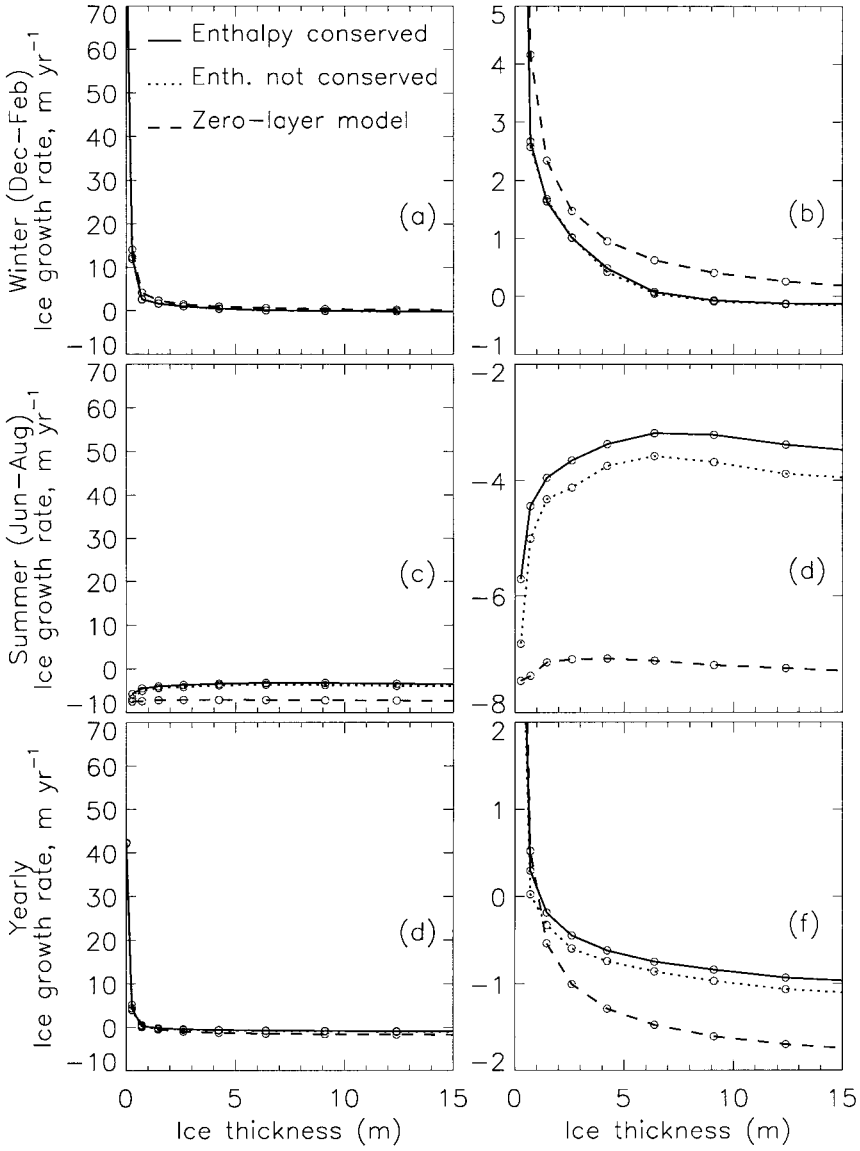

FIG. 8. Simulated mean ice growth rate versus ice thickness. The left panels have the same large vertical range; the right panels have different small vertical ranges. The ice growth rates for ice thicker than 15 m are not plotted.

the three-layer models for 0–0.4 m ice, and the difference in ice growth rate between the two three-layer models with or without conserving ice enthalpy is generally within the range of 1 m yr^{-1} (Fig. 8), which is not discernible in Fig. 9a.

For ice thicker than 0.4 m, the melt season increases to about 4 months (Figs. 9b–9f) because of the effect of heat conduction in the ice. The difference in growth rate among the models becomes conspicuous now that the growth rates are considerably smaller than those for very thin ice. Again, the melt rates calculated by the zero-layer model are much larger than those calculated by the other two models, while the melt rates calculated by the nonconservative model are slightly larger than those calculated by the full model. The exaggeration of seasonal variability by the zero-layer model (Fig. 6) is prominently reflected in the behavior of the predicted growth and melt rates. In addition, the timing of ice thaw and freeze-up estimated by the zero-layer model is considerably different from that estimated by the other two models except for 0.4–2 m ice (Fig. 9b). The nonconservative model, on the other hand, differs from the full model only in the timing of ice freeze-up for 0.4–5 m ice (Figs. 9b and c), delaying the fall ice freeze-up by about 6 days. For very thick ice (11–28 m), the two models that use the three-layer thermodynamic scheme hardly predict any ice growth all year round, whereas the zero-layer model estimates

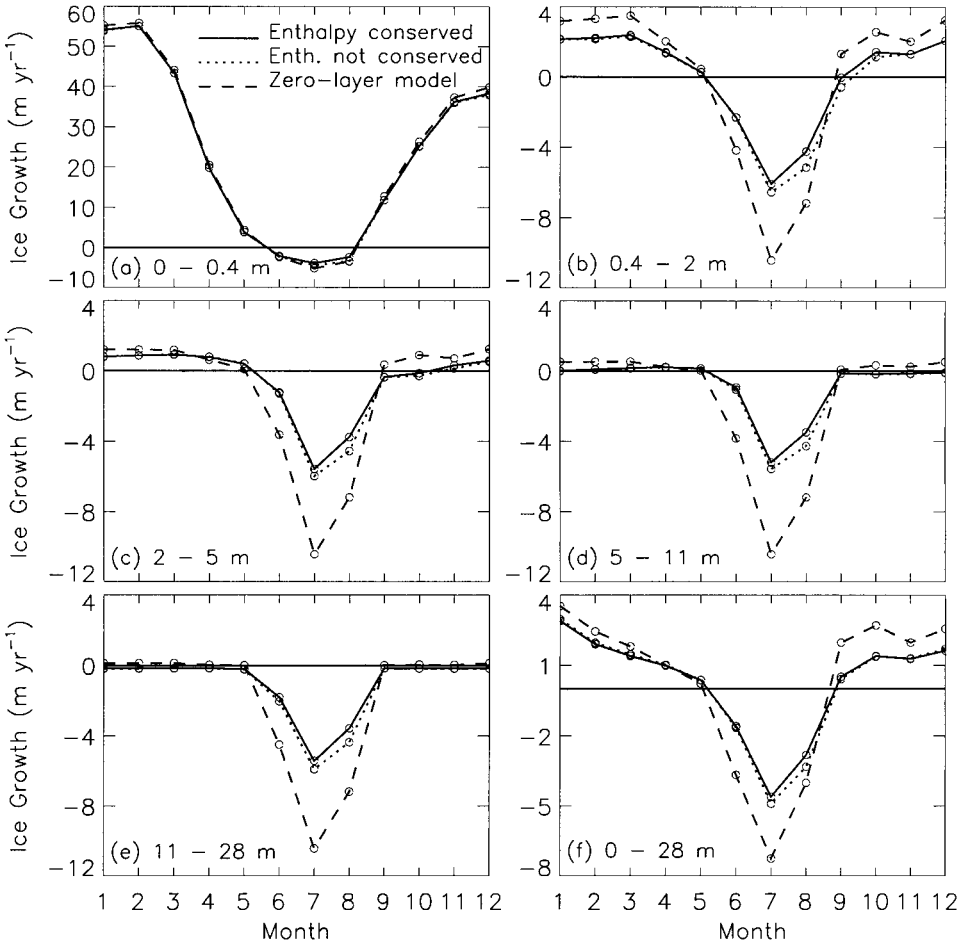

FIG. 9. Simulated monthly variations in mean ice growth rate for different ice thickness ranges.

ice growth in winter, early spring, and fall regardless of ice thickness.

Another feature shown in Fig. 9 is that the nonconservative model generally estimates melt rates slightly elevated from the enthalpy-conserving model in several months after June. This is linked to the fact that the nonconservative model estimates a lower aggregate surface albedo than the full model for the same period (Figs. 10a and 10b). In fact, the higher ice melt and the lower surface albedo are closely related to the surface albedo feedback; that is, the increased ice melt reduces mean ice thickness by increasing 1–2 m ice and decreasing the ice thicker than 2 m in comparison with the full model (Fig. 7c). During summer melting, the 1–2 m ice is easily turned into open water or very thin ice (0–0.4 m). As a result, a larger area of open water and very thin ice is created by the nonconservative model (Fig. 7d), which lowers the summer surface albedo (Figs. 10a and 10b). The reduced albedo in turn allows more absorption of solar radiation at the surface (Figs. 10c and 10d) and therefore further enhances ice melt. Clearly, this is an effect of the positive surface albedo feedback.

The zero-layer model, on the other hand, underestimates the surface albedo more significantly during that period (Figs. 10a and 10b). This is because of the same surface albedo feedback that links the excessive ice melt to an excessive absorption of solar radiation at the surface (Figs. 10c and 10d). Note that the excessive solar absorption not only leads to an excessively rapid ice melt but also to an excessively rapid snow melt. In fact, the snow is melted so much that its build-up is delayed by almost one month (Fig. 10e), which further reduces the surface albedo. This shows that use of different thermodynamic models, whether allowing heat storage in ice or whether conserving ice enthalpy, not only affects the simulation of ice but also affects the simulation of other physical variables in the snow–ice system in which the well-established surface albedo feedback mechanism plays a prominent role.

c. Ice temperatures

We have described the likely linkage between the surface albedo feedback and the nonconservative model's overestimation of ice melt and underestimation of

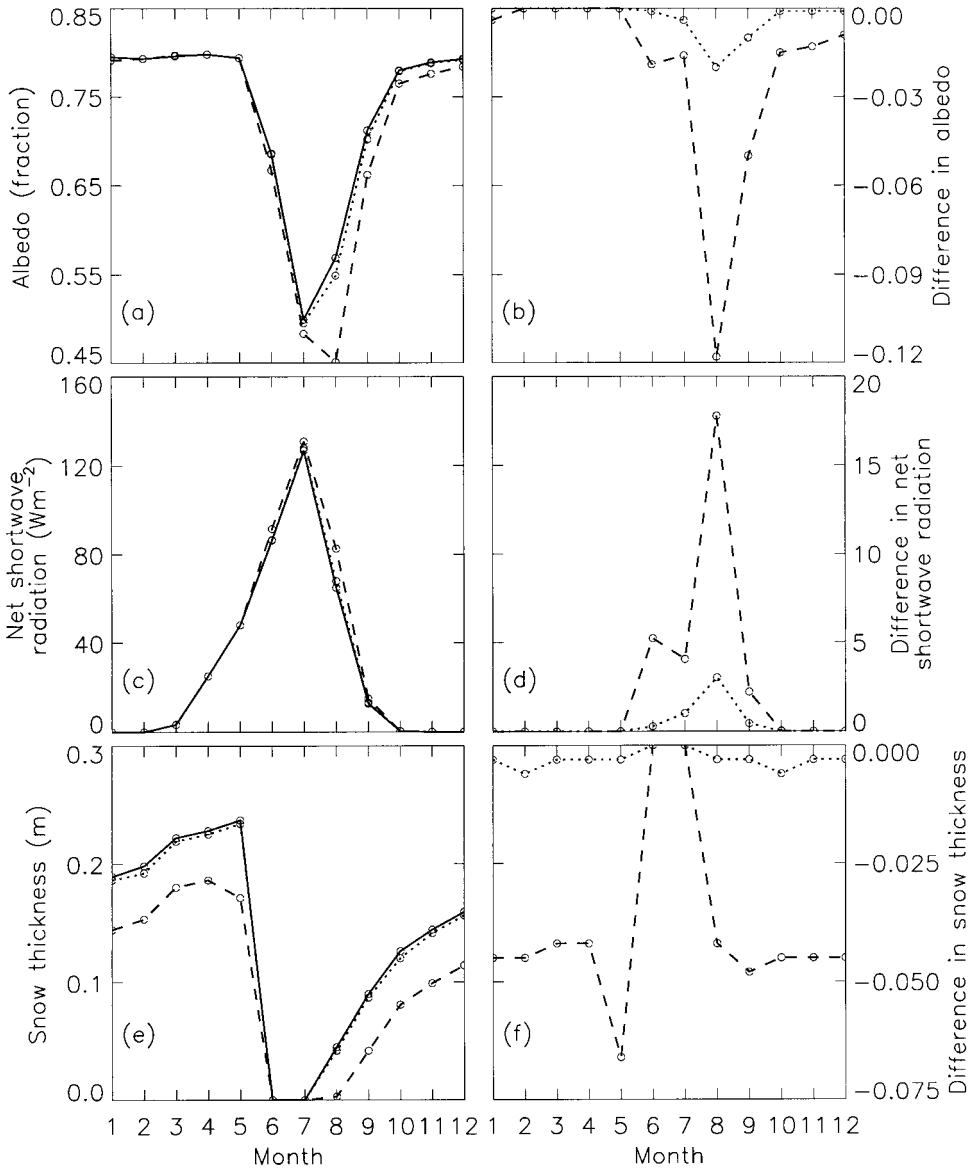

FIG. 10. Simulated mean (a) surface albedo, (b) difference in surface albedo, (c) net shortwave radiation at the surface, (d) difference in net shortwave radiation, (e) snow thickness, and (f) difference in snow thickness. The solid line is for the full model, the dotted line is for the nonconservative model or for the nonconservative model minus the full model, and the dashed line is for the zero-layer model or for the zero-layer model minus the full model.

ice thickness. However, since the nonconservative model only differs from the full model in its inability to conserve ice enthalpy for various sea ice processes, we expect that this model deficiency is the original source of bias and is likely to manifest with the simulated ice interior temperatures. Seasonal snapshots of the temperatures within the two ice layers (Fig. 11) show that the temperatures in both the upper and lower layers vary substantially with ice thickness. They are also subject to considerable seasonal variability, particularly for 0–15 m ice. However, for the thickest ice (>20 m), the lower-layer temperature is more or less close to the freezing temperature of seawater (−1.96°C), and the upper-layer temperature is between the freezing temperature of seawater and the melting temperature of ice (specified as −0.11°C). They also exhibit less seasonal variability. This indicates that the surface conditions have less impact on the temperatures in the deep interior of very thick ice. For most ice thicknesses, the lower layer is warmer than the upper layer except for July through September. One notable feature is that, with every passing day, the coldest temperature in each layer moves, at a different pace, toward thicker ice. In November, the coldest up-

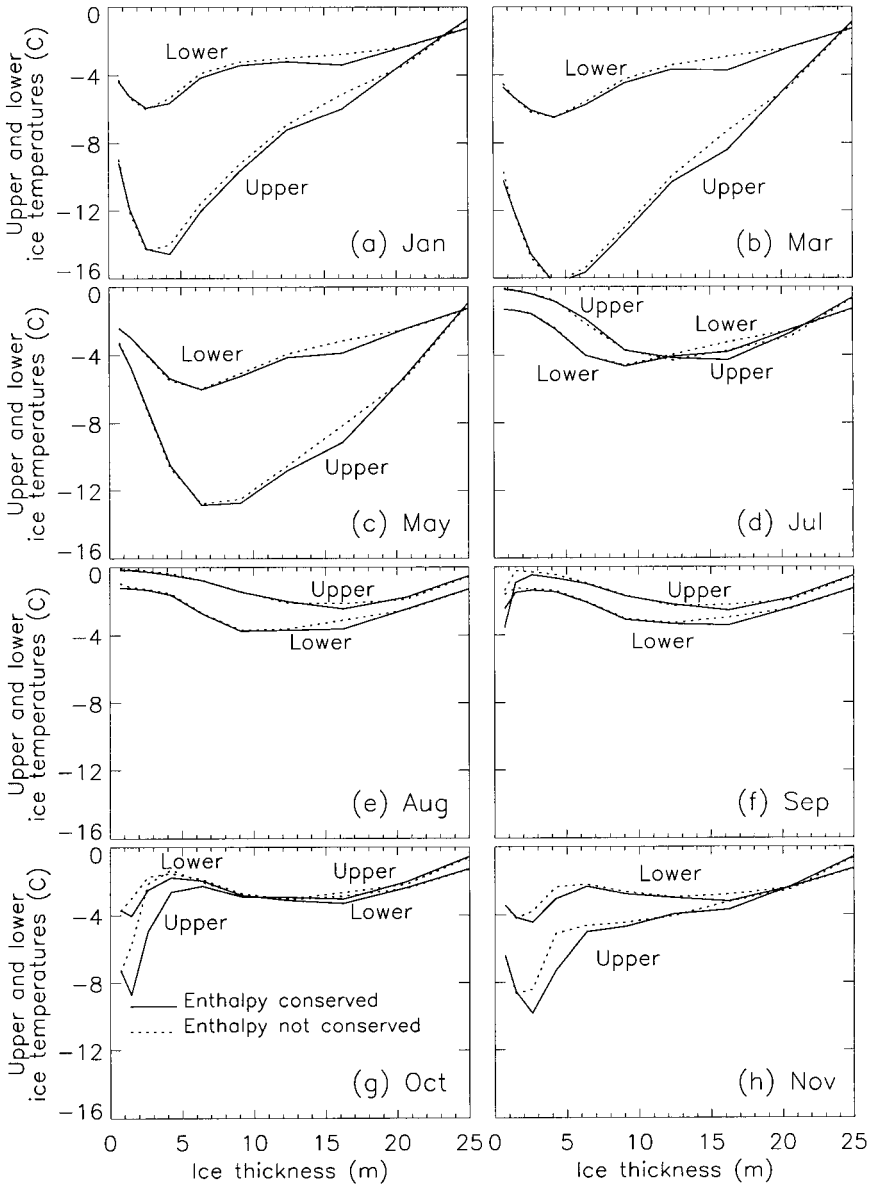

FIG. 11. Simulated seasonal evolution of temperatures in the upper and lower ice layers.

per and lower temperatures occur almost simultaneously in 2–3 m ice. They move to about 4-m ice in March. By July, the coldest temperature in the upper layer occurs in ice about 15 m thick, while the coldest temperature in the lower layer occurs in ice about 9 m thick. This represents the annual cold wave from the atmosphere, chilling and penetrating the ice.

The implementation of (5) and the conservation of ice thermal energy affect the prediction of the temperatures within the ice. As shown in Fig. 11, the temperatures estimated by the full model for both the upper and lower layers are generally lower than those estimated by the nonconservative model for 3–18 m ice. An interesting feature is that after summer the temperatures estimated by the full model for both the upper and lower layers become significantly lower for 0–5 m ice in September (Fig. 11f), for 1–6 m ice in October (Fig. 11g), and for 2–8 m ice in November (Fig. 11h). This suggests that the ice temperatures estimated by the enthalpy-conserving model become progressively lower for 0–8 m ice as time progresses after summer. This is because the implementation of (5) causes a redistribution of enthalpy from thin ice categories to thick ones in the event of active ice growth and ridging after a summer of ice decay. In September, the minimum ice temperatures, driven by atmospheric forcing, occur in the very thin ice, and the transfer of thin ice into thicker ice reduces the temperatures in 0–5 m ice. In October,

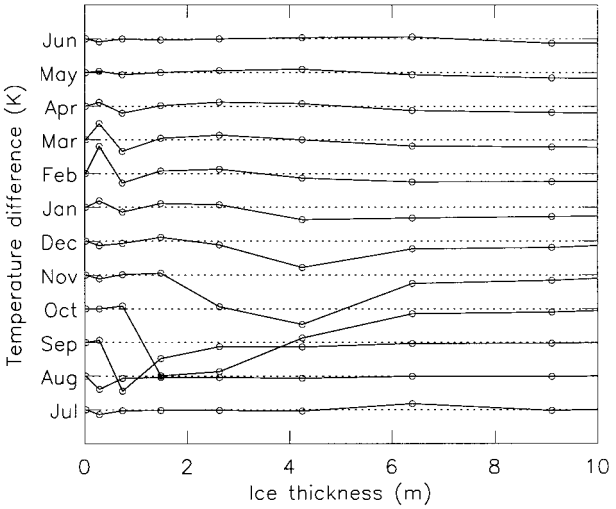

FIG. 12. Evolution of the differences in the upper ice temperature between enthalpy-conserving model and the nonconservative model (the enthalpy-conserving model minus the nonconservative model). The differences (in solid line) are shown over a one-year cycle starting from Jul. The dotted lines are zero-difference lines. The interval between ticks on the vertical axis represents 1.5 K.

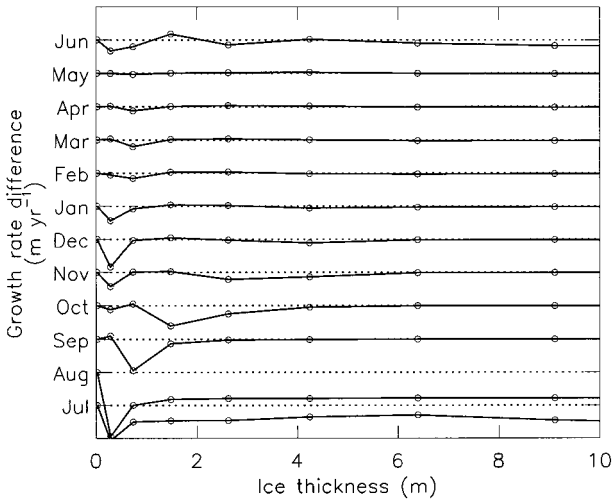

FIG. 13. Evolution of the difference in ice growth rate between the nonconservative model and the enthalpy-conserving model (the nonconservative model minus the enthalpy-conserving model). The difference (in solid line) is shown over a one-year cycle starting from Jul. The dotted lines are zero-difference lines. The interval between ticks on the vertical axis represents 1 m yr^{-1}.

the minimum temperatures occur in 1-m ice and the continuing transfer of thin ice into thicker ice reduces the temperatures in 1–6 m ice. In November, the minimum temperatures occur in 2–3 m, and the temperatures are lower in 2–8 m ice. This is why the temperature estimated by the full model is progressively lower for the 0–8 m ice, where the ice transfer is most active and therefore the enthalpy redistribution appears to be most noticeable.

The transfer of ''cold'' to thicker ice by thermodynamic growth and mechanical ridging in fall is further illustrated in Fig. 12, which plots the differences in the upper ice temperature between the full model and the nonconservative model over 0–8 m ice (the first 8 ice categories). The differences are shown over a one-year cycle starting from July. In July, the difference is small. In August, the difference trough at category 2 deepens, indicating an intensification of enthalpy redistribution driven by an increasing ice growth and ridging. The trough then moves to category 3 in September, to category 5 in October, and to category 6 in November. It reaches the maximum in depth in October at category 5 and then flattens, gradually spreading over a larger thickness range and moving toward ice thicker than 8 m in the following months. This shows a clear after-summer enthalpy redistribution given that the differences in the lower temperature between the enthalpy-conserving model and the nonconservative model are similar with smaller amplitude (not shown).

The enthalpy redistribution from thin to thicker ice in fall impacts ice growth, as shown in Fig. 13, which plots the difference of ice growth rates between the nonconservative model and the enthalpy-conserving model. In both July and August, the nonconservative model considerably overpredicts ice melt rates over all ice thicknesses, which, as mentioned before, is linked to a decrease in surface albedo (Figs. 10a and 10b). In these two months, the growth-rate differences have a trough at ice category 2. In the following months, from September to November, the trough of the growth-rate difference follows the peak of the temperature differences as the ice enthalpy redistributes. This is because the progressively elevated ice interior temperatures in fall, simulated by the nonconservative model, affect the heat convergence or divergence at the surface or the bottom of the ice by changing the heat conduction in the ice. This leads to lower ice growth rates in fall (Figs. 9 and 13). It also leads to a delay of fall ice freeze-up over 0.4–5 m ice (Figs. 9b and 9c).

Although the enthalpy transfer may continue in thicker ice after fall, Fig. 12 hardly shows a continuing enthalpy redistribution over 0–5 m ice, which may indicate that the enthalpy transfer from thin ice to thicker ice after fall is not significant in that thickness range. From December to March the temperature differences have a peak at ice category 2 and, at the same time, a trough at category 3. We do not exactly know what causes that. Meanwhile, the growth-rate differences have a trough at category 2 in November through January. Apparently, the linkage between the growth rates and the ice temperatures is not as strong in other seasons as in fall. Nevertheless, we may still attribute the nonconservative model's bias in predicting ice thickness ultimately to its inability to transfer and conserve ice enthalpy, based on the linkage between its elevated ice temperatures and suppressed ice growth in fall. That is, the model's failure to transfer and conserve ice enthalpy leads to warmer ice interior temperatures progressively over 0–8 m ice

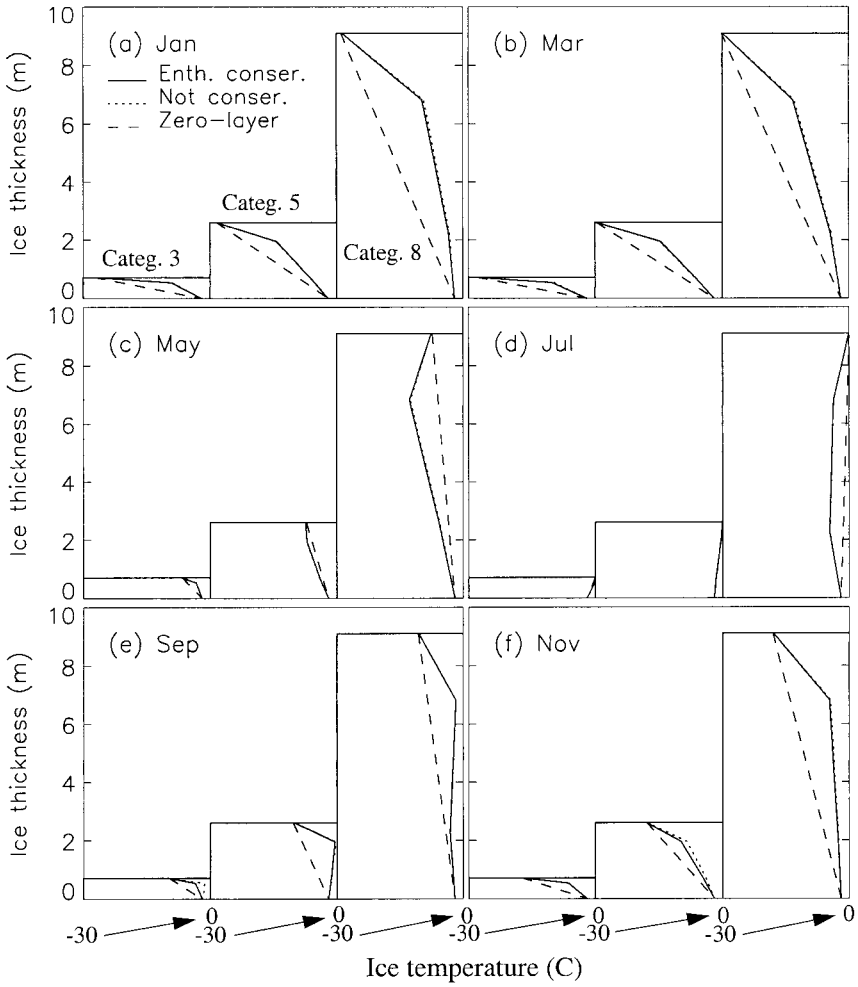

FIG. 14. Simulated seasonal evolution of the vertical temperature profile in the ice for three selected ice categories: category 3 (0.4–1.0 m), 5 (1.9–3.3 m), and 8 (7.6–10.6 m). When not visible, the curve for the nonconservative model is hidden from that for the full model.

in comparison with the full model (Figs. 11 and 12); the warmer ice temperatures lead to a suppressed ice growth in fall (Figs. 9 and 13); the suppressed ice growth leads to a larger area of 1–2 m ice (Fig. 7c), which leads to a larger area of open water and very thin ice (0–0.4 m) during summer melting (Fig. 7d); a larger area of open water and very thin ice leads to a lower average surface albedo and stronger absorption of solar radiation at the surface, which enhances ice melt in summer. Such a sequence, we believe, causes the nonconservative model to underestimate ice thickness.

The seasonal evolution of the vertical temperature profiles for three selected ice categories is shown in Fig. 14. Unlike the linear profiles calculated by the zero-layer model, the profiles calculated by the two models with a three-layer thermodynamic scheme are characterized by a strong nonlinearity (i.e., considerable curvature in the profile), except in summer over relatively thin ice. The strong seasonal variability in the curvature of the profile illustrates how the heat or cold stored in ice affects ice growth and melt. The transfer of ice enthalpy in fall is again reflected in Figs. 14e and 14f, which show noticeably warmer temperatures for the nonconservative model at ice category 3 in September and at category 5 in November. This small difference in temperature profiles gives rise to a considerable difference in mean thickness (Fig. 5).

Figure 14 illustrates well why the zero-layer model exaggerates the seasonal variability of ice thickness with an overestimation of ice melt in summer and an overestimation of ice growth in other seasons. In fall, winter, and early spring, the zero-layer model's linear temperature profile has a larger temperature gradient at the ice bottom, which conducts more heat upward and therefore exaggerates ice growth (Figs. 14a, 14b, 14e, and 14f). In late spring and summer, the zero-layer model uses all the downward heat flux from the surface to melt ice, while the three-layer models use a portion of the downward heat flux to warm the ice (Figs. 14c and 14d).

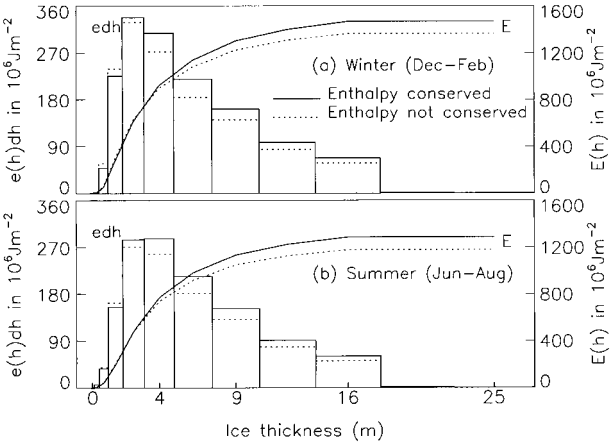

FIG. 15. Simulated mean enthalpy distribution (histogram) and cumulative enthalpy distribution (monotonically increasing curve).

d. Enthalpy distribution

Figure 15 shows the simulated enthalpy distribution, $e(h)dh$, and cumulative enthalpy distribution, $E(h)$. As mentioned before, the enthalpy distribution function is not a normalized function, nor is the cumulative function. However, they describe how much enthalpy the ice possesses and how the enthalpy is distributed over different ice categories. Also note that the calculation of ice enthalpy is referenced to zero absolute temperature ($T = 0$ K) so that enthalpy is always positive. In either winter or summer, most of the ice enthalpy is stored in ice categories 5 and 6 (2–4 m thick) although most of the ice is concentrated in categories 4 and 5 (2–3 m thick; Fig. 7). This is because the amount of ice enthalpy is proportional to both ice thickness and concentration. The ice in category 4 has relatively large concentration, but it is thin and therefore contains less enthalpy. As the ice becomes thicker, its enthalpy per unit area becomes larger, but its concentration decreases more rapidly. As a result, the amount of enthalpy decreases for thick ice categories. Comparing Figs. 15a and 15b, we see that the winter ice has more enthalpy than the summer ice (this is shown more clearly by the cumulative distribution), although the summer ice is warmer than the winter ice (Figs. 11 and 14). This is because winter has more ice than summer has. Compared to the nonconservative model, the full model generally estimates more enthalpy for ice thicker than 2 m and less enthalpy for ice thinner than 2 m. This is because the former calculates more ice thicker than 2 m and, at the same time, less ice thinner than 2 m (Fig. 7). Overall, the total enthalpy simulated by the full model is larger than that simulated by the nonconservative model. This is attributed to the fact that the nonconservative model, although predicting warmer ice interior temperatures, underestimates ice thickness, which indicates that the changes in ice thickness distribution g are more influential on changes in enthalpy distribution e.

e. Sensitivity to input forcing

How do the models react to changes in the input forcing? To examine the behavior of the three models in response to changes in thermal and mechanical forcing, we conducted two series of sensitivity studies in which the model forcing was moderately changed. In the first series, the downward shortwave radiation (Fig. 4c) was proportionally increased or decreased by 5%, while the rest of the forcing remained the same. In the second series, the ice shear (Fig. 4e) was proportionally increased or decreased by 25%.

The models' responses to the perturbations of shortwave radiation are shown in Table 1, and responses to the perturbations of ice shear in Table 2; only the 50th-yr mean ice thicknesses are listed in the two tables. As can be seen, the models are more or less sensitive to the perturbations in input forcing. Within the range of thermal and mechanical perturbations used in the study, the ice thickness estimated by the full model is consistently about 10% larger than that estimated by the nonconservative model. Although the nonconservative model and zero-layer model do not differ much in annual mean ice thickness, they do in seasonal variability of thickness, as shown for the standard case in Fig. 6.

We have also tested these three models using the atmospheric forcing data for 1993. The model behaviors illustrated in Figs. 5 and 6 are essentially the same for 1993 (not shown). All these sensitivity runs lead us to believe that, under moderately different dynamic and thermodynamic conditions, the behavior of these models, relative to each other, would remain more or less the same.

5. Concluding remarks

The theory of sea ice thickness distribution developed by Thorndike et al. (1975) has been extended to include enthalpy distribution. The extended theory conserves both ice mass and ice thermal energy by jointly solving a thickness-distribution equation and an enthalpy-distribution equation. Both equations have been implemented into a dynamic thermodynamic sea-ice model with 12 ice thickness categories following the numerical procedure of Hibler (1980). The implementation of the enthalpy-distribution equation makes it possible to replace the zero-layer thermodynamic model of Semtner (1976), adopted in the Hibler (1980) sea-ice model, with more realistic thermodynamic models, such as the three-layer thermodynamic models of Semtner (1976) and Winton (2000) or the general multilayer model of Maykut and Untersteiner (1971) and its variants. Unlike the zero-layer thermodynamic model, a three-layer or a multilayer model allows the sea ice to store heat. The thermal energy stored in the ice is subject to changes owing to dynamic and thermodynamic sea-ice processes. These changes can be tracked by the enthalpy-distribution equation in order to conserve thermal energy. Conse-

TABLE 1. Effect of a 5% perturbation in input downward shortwave radiation on 50th-yr mean ice thickness.

	Standard +5%	Standard	Standard −5%
Enthalpy-conserving model	2.09	2.79	3.41
Nonconservative model	1.86	2.52	3.23
Zero-layer model	1.67	2.45	3.02

TABLE 2. Effect of a 25% perturbation in input ice shear on 50th-yr mean ice thickness.

	Standard −25%	Standard	Standard +25%
Enthalpy-conserving model	2.64	2.79	2.93
Nonconservative model	2.38	2.52	2.63
Zero-layer model	2.37	2.45	2.52

quently the thickness- and enthalpy-distribution sea-ice model is able to conserve not only ice mass but also ice thermal energy in the presence of ice advection, growth or decay, lateral melting, and ridging.

The performance of the combined thickness- and enthalpy-distribution sea-ice model was examined with a one-dimensional model configuration incorporating the Winton (2000) three-layer thermodynamic scheme and was driven by observed daily thermodynamic forcing and modeled daily kinematic forcing. The model was able to capture the basic features of the seasonal variability in ice growth or decay and ice thickness distribution for ice of a variety of thicknesses. It was also able to shed light on the behavior of the temperature in the interior of the ice and the enthalpy distribution over different ice types in response to seasonal variations in thermal forcing at ice surface. Because of the implementation of the enthalpy-distribution equation, the model allows ice enthalpy, or the heat stored in the ice, to propagate after summer, driven by an active ice growth and ridging, in order to conserve energy. The simulated strong seasonal variability in the heat stored in the ice is reflected by the evolution of the nonlinear vertical ice temperature profile. The seasonally varying heat stored in the ice regulates the surface cooling and heating through heat conduction in the ice and therefore significantly affects the model's estimate of ice growth and decay, the timing of ice thaw and freeze-up, and the prediction of the seasonal evolution of ice.

Parallel to the integration of the full thickness- and enthalpy-distribution model, a second model was run in which the enthalpy-distribution equation was not implemented and therefore ice thermal energy was not conserved during processes such as advection, growth, and ridging. The results indicate that not conserving thermal energy has a noticeable impact on the prediction of the interior temperature of the ice or the heat stored in the ice. This is particularly so in fall because of the model's inability to redistribute ice enthalpy. The inability to propagate and conserve ice enthalpy affects the model's response to surface cooling and heating and therefore the model's calculation of ice growth and, particularly, summer ice melt, in such a way that involves the positive surface albedo feedback. Specifically, such an inability leads to a warmer ice interior temperature or more heat storage in ice, which reduces ice growth in fall. The reduced ice growth leads to a larger area of open water and thin ice during summer melting, which lowers the surface albedo, invites more solar radiation, and therefore causes more ice melt. As a result, the nonconservative model, in comparison with the enthalpy-conserving model, underestimates ice thickness by 11% under various conditions of thermal and mechanical forcing. This stresses the importance of solving the enthalpy-distribution equation in order to conserve thermal energy in the ice in numerical investigations of climate. Conserving thermal energy to eliminate the 11% bias is also helpful for model–data comparisons in an era when excellent ice thickness observations are available (Rothrock et al. 1999).

A third model was run that used a zero-layer scheme to compare the results of a simplified thermodynamic model. The zero-layer model tended to substantially exaggerate the seasonal variability in ice of a variety of thicknesses. Semtner (1976) found such an exaggeration for ice about 3 m thick. It appears to exist with ice of many different thicknesses. The zero-layer model also significantly overestimated the seasonal variability of many other quantities, such as the ice interior temperature, ice growth, decay, and surface albedo, for various ice thicknesses. These overestimations were all closely linked and were responsible for the overprediction of the seasonal variation in ice thickness.

Finally, we want to point out that the numerical implementation of the enthalpy-distribution equation is not computer demanding. It takes only about 15% of the computer time for the entire thermodynamic calculation. Also, since the thickness- and enthalpy-distribution sea-ice model is based on Eulerian equations [(1) and (5)], the redistributor, $\gamma(h', h)$, is time independent and does not need to be updated at each model time step and at each model grid cell. Consequently, the calculation of changes in both the thickness distribution and the enthalpy distribution due to ridging is not time consuming, an important attribute for global climate modeling or fine-resolution regional climate modeling.

Acknowledgments. This work was supported by NASA Grant NAG5-4375 (for an EOS interdisciplinary Investigation, POLar Exchange at the Sea surface), ONR Grant N00014-99-1-0742, and NOAA Grant NA76GP0508. We thank G. A. Maykut for helpful suggestions, I. G. Rigor for providing sea level pressure and surface air temperature data, and M. Ortmeyer for computer assistance.

REFERENCES

Arbetter, T. E., J. A. Curry, and J. A. Maslanik, 1999: Effects of rheology and ice thickness distribution in a dynamic–thermodynamic sea ice model. *J. Phys. Oceanogr.,* **29,** 2656–2670.

Bitz, C. M., M. M. Holland, A. J. Weaver, and M. Eby, 2001: Simulating the ice-thickness distribution in a coupled climate model. *J. Geophys. Res.,* **106,** 2441–2463.

Bjork, G., 1992: On the response of the equilibrium thickness distribution of sea ice to ice export, mechanical deformation, and thermal forcing with application to the Arctic Ocean. *J. Geophys. Res.,* **97,** 11 287–11 298.

Ebert, E. E., and J. A. Curry, 1993: An intermediate one-dimensional thermodynamic sea ice models for investigating ice–atmospheric interactions. *J. Geophys. Res.,* **98,** 10 085–10 109.

Flato, G. M., and W. D. Hibler III, 1995: Ridging and strength in modeling the thickness distribution of Arctic sea ice. *J. Geophys. Res.,* **100,** 18 611–18 626.

——, and R. D. Brown, 1996: Variability and climate sensitivity of landfast Arctic sea ice. *J. Geophys. Res.,* **101,** 25 767–25 777.

Hibler, W. D., III, 1979: A dynamic thermodynamic sea ice model. *J. Phys. Oceanogr.,* **9,** 815–846.

——, 1980: Modeling a variable thickness sea ice cover. *Mon. Wea. Rev.,* **108,** 1943–1973.

Martin, S., and E. A. Munoz, 1997: Properties of the Arctic 2-meter air temperature field for 1979 to the present derived from a new gridded data set. *J. Climate,* **10,** 1428–1440.

Maykut, G. A., and N. Untersteiner, 1971: Some results from a time-dependent thermodynamic model of sea ice. *J. Geophys. Res.,* **76,** 1550–1575.

Parkinson, C. L., and W. M. Washington, 1979: A large-scale numerical model of sea ice. *J. Geophys. Res.,* **84,** 311–337.

Randall, D., and Coauthors,1998: Status of and outlook for large-scale modeling of atmosphere–ice–ocean interactions in the Arctic. *Bull. Amer. Meteor. Soc.,* **79,** 197–219.

Rigor, I. G., R. L. Colony, and S. Martin, 2000: Variations in surface air temperature observations in the Arctic, 1979–97. *J. Climate,* **13,** 896–914.

Rothrock, D. A., Y. Yu, and G. A. Maykut, 1999: Thinning of the arctic sea-ice cover. *Geophys. Res. Lett.,* **26,** 3469–3472.

Schramm, J. L., M. M. Holland, and J. A. Curry, 1997: Modeling the thermodynamics of a sea ice thickness distribution, 1. Sensitivity to ice thickness resolution. *J. Geophys. Res.,* **102,** 23 079–23 091.

Semtner, A. J., Jr., 1976: A model for the thermodynamic growth of sea ice in numerical investigations of climate. *J. Phys. Oceanogr.,* **6,** 379–389.

Steele, M., and G. Flato, 2000: Sea ice growth, melt, and modeling: A survey. *The Freshwater Budget of the Arctic Ocean,* E. L. Lewis and E. P. Jones, Eds., Kluwer, 549–587.

Thorndike, A. S., D. A. Rothrock, G. A. Maykut, and R. Colony, 1975: The thickness distribution of sea ice. *J. Geophys. Res.,* **80,** 4501–4513.

——, R. Colony, and E. Munoz, 1983: Arctic Ocean buoy program, data report. Applied Physics Laboratory, University of Washington, Data Report 132 pp.

Vowinckel, E., and S. Orvig, 1970: The climate of the North Polar Basin. *World Survey of Climatology.* Vol. 14, *Climates of the Polar Regions,* S. Orvig, Ed., Elsevier, 1–37.

Winton, M., 2000: A reformulated three-layer sea ice model. *J. Atmos. Oceanic Technol.,* **17,** 525–531.

Zhang, J., and W. D. Hibler III, 1997: On an efficient numerical method for modeling sea ice dynamics. *J. Geophys. Res.,* **102,** 8691–8702.

——, ——, M. Steele, and D. A. Rothrock, 1998a: Arctic ice-ocean modeling with and without climate restoring. *J. Phys. Oceanogr.,* **28,** 191–217.

——, D. A. Rothrock, and M. Steele, 1998b: Warming of the Arctic Ocean by a strengthened Atlantic inflow: Model results. *Geophys. Res. Lett.,* **25,** 1745–1748.

——, ——, and ——, 2000: Recent changes in Arctic sea ice: The interplay between ice dynamics and thermodynamics. *J. Climate,* **13,** 3099–3114.